Observation of a long-time tail in Brownian motion

1981 J. Phys. A: Math. Gen. 14 3301

(http://iopscience.iop.org/0305-4470/14/12/025)

J. Phys. A: Math. Gen. **14** (1981) 3301–3327. Printed in Great Britain

Observation of a long-time tail in Brownian motion

G L Paul† and P N Pusey

Royal Signals and Radar Establishment, Malvern, Worcestershire, WR14 3PS, England

Received 28 April 1981

Abstract. By photon correlation dynamic laser light scattering we have measured the time dependence of the mean-square displacement $\langle \Delta x^2(t) \rangle$ of spherical particles (radius $\sim 1.7\ \mu$m) in Brownian motion. Clear evidence was found for the existence of a $t^{1/2}$ term in $\langle \Delta x^2(t) \rangle$ which corresponds to the expected $t^{-3/2}$ 'long-time tail' in the particle velocity autocorrelation function. The experimentally determined amplitude of the $t^{1/2}$ term was about $74 \pm 3\%$ of the value predicted theoretically. Despite detailed consideration of possible systematic errors we were unable to explain the magnitude of this disagreement.

1. Introduction

Until about 15 years ago it was widely thought that microscopic processes (such as velocity fluctuations) and macroscopic processes (such as diffusion) in fluid systems were associated with well separated timescales. Doubt was cast on this viewpoint by the molecular dynamics computer 'experiments' of Alder and Wainwright (1967, 1968, 1970) which showed a slow, $t^{-3/2}$, asymptotic decay in the velocity autocorrelation function of an atom in a hard-sphere fluid. Qualitatively this observation was explained in terms of the slowly developing viscous flow pattern (which could be described by macroscopic hydrodynamics) in the fluid surrounding the atom in question (Alder and Wainwright 1970, Zwanzig and Bixon 1970). In the years since this discovery such 'long-time tails' in correlation functions of microscopic properties have appeared in many theories (see Pomeau and Résibois 1975 for a review) and their existence has become generally accepted among statistical physicists. Nevertheless real (as opposed to computer) experimental evidence for these slow decays remains remarkably sparse. Indications of their existence have been found in neutron scattering by simple liquids (Andriesse 1970, Carneiro 1976, Bosse *et al* 1979) and in the direct observation of the movement of microscopic particles, either after acceleration by a shock wave (Kim and Matta 1973) or in natural Brownian motion (Fedele and Kim 1980). Also Bouchiat and Meunier (1971, 1972) have observed the effects of slow bulk velocity correlations on the thermally excited vibrations of a free liquid surface (see also Zollweg *et al* 1971, Nelkin 1972). Early in the development of the subject it was realised that the technique of dynamic light scattering offered promise for the detection of a long-time tail in the velocity autocorrelation function of spherical particles in Brownian motion (B J Berne 1971 private communication, Nelkin 1972, Harris 1975). Because of various experimental difficulties there has, to date, been only one successful experiment on these lines. Boon and Bouiller (1976) (also Bouiller *et al* 1978) reported an effect of the magnitude predicted theoretically; however the statistical error in their measurements was large, about half the size of the effect itself.

† On leave from the University of New South Wales, Sydney, Australia.

0305-4470/81/123301+27$01.50

Here we report a measurement similar to, but much more precise than, that of Boon *et al.* In these experiments the detectability of the long-time tail is determined largely by the ratio $\rho R/\eta^2$ where R is the particle radius, ρ the density of the suspending fluid and η its shear viscosity (§ 2.3). The increased precision of our experiment compared with that of Boon *et al* stems from three factors: (i) the use of much larger spheres (radius ~ 1.7 μm compared with 0.088 μm), (ii) measurements made at much shorter times compared with the characteristic decay time of the light scattering correlation function, where the effect sought is larger, (iii) long experimental accumulation times (as much as a day in some cases).

For various reasons, dynamic light scattering experiments on spheres of radius 0.5 μm or more are notoriously difficult. Because the size distribution of our spheres was extremely narrow (§ 3.1), problems associated with the size dependence of the angular scattering intensity profile were avoided. In preliminary experiments the main problem was found to be correlated motions of the particles due to residual convective flows in the suspending fluid and, possibly, sedimentation. In the final experiments convection was minimised by using a small sample volume (1×0.2 cm^2 cross section by less than 1 cm high) and immersing the sample cell in a 3 l water bath. Sedimentation was reduced by (nearly) matching the density of the fluid ($H_2O + D_2O$) to that of the particles (~ 1.055 g cm^{-3}).

Our results (figures 3 and 4) clearly support the existence of a negative $t^{1/2}$ term in the mean-square displacement of a Brownian particle corresponding to a $t^{-3/2}$ tail in its velocity autocorrelation function. While the magnitude of this term was about 25 times greater than the estimated statistical error in its measurement, it was only about $74 \pm 3\%$ of the value predicted theoretically (see table 6, last column). By contrast, the long-time diffusion coefficient of the particle, measured by dynamic light scattering, was found to be about $4 \pm 2\%$ smaller than the value calculated from the particle size. This latter discrepancy indicates the presence of some (relatively small) systematic error in the measurements. However, despite detailed consideration of possible sources of systematic error (§ 6), we were unable to explain the much larger discrepancy, mentioned above, between the experimentally found and theoretically predicted magnitudes of the long-time tail (see § 7 for further discussion).

In the next section we outline the theory of both the light scattering measurement and of the velocity autocorrelation function and mean-square displacement of a Brownian particle. Experimental details are given in § 3. Section 4 is devoted to presentation of the results which show long-time tail effects most clearly whereas in § 5 details of supplementary experiments, necessary for validation of our approach to the problem, are given. In the main these latter experiments corroborate those of § 4 though some minor inconsistencies remain unresolved. In § 6 we consider in detail possible sources of systematic error which include distortions in the electronic signal processing, convection and sedimentation, heterodyning, number fluctuations, dust, multiple scattering, wall effects and interparticle interactions. Our conclusions are summarised in § 7. Sections 5 and 6 could be omitted by a casual reader.

2. Theory

2.1. Light scattering

Photon correlation dynamic light scattering (for reviews see Cummins and Pike 1974, 1977) provides an experimental estimate of the normalised temporal autocorrelation

function $g^{(2)}(\tau)$ of the scattered light intensity I:

$$g^{(2)}(\tau) = \langle I(0)I(\tau)\rangle / \langle I\rangle^2. \tag{2.1}$$

Here τ is the correlation delay time and the angular brackets indicate time or ensemble averages. If the light is scattered by a large number of particles, its field amplitude is a complex Gaussian random variable and

$$g^{(2)}(\tau) = 1 + c(g^{(1)}(\tau))^2 \tag{2.2}$$

where c is an apparatus constant of order one determined by spatial coherence, signal to dark count ratio, etc. If the particles are identical, spherical and non-interacting the field correlation function $g^{(1)}(\tau)$ is just the so-called self intermediate scattering function

$$g^{(1)}(K, \tau) = \langle \exp \mathrm{i}\, K \Delta x(\tau)\rangle \tag{2.3}$$

where K is the magnitude of the scattering vector

$$K = (4\pi/\lambda_0) n \sin \tfrac{1}{2}\theta, \tag{2.4}$$

λ_0 being the wavelength of the light *in vacuo*, n the refractive index of the particle suspension and θ the scattering angle. The particle displacement $\Delta x(\tau)$ is given by

$$\Delta x(\tau) = \int_0^\tau \mathrm{d}t\, v(t) \tag{2.5}$$

where $v(t)$ is one Cartesian component of particle velocity; the average particle motions are assumed to be isotropic. If the random forces (§ 2.2), due to the suspending fluid, which drive the particle motion have Gaussian statistics it follows that $v(t)$ and hence $\Delta x(\tau)$ are also zero-mean Gaussian-distributed variables (e.g. Dufty 1974, Fox 1977). Then (2.3) becomes (e.g. Davenport and Root 1958)

$$g^{(1)}(K, \tau) = \exp(-\tfrac{1}{2}K^2 \langle \Delta x^2(\tau)\rangle) \tag{2.6}$$

and a measurement of $g^{(2)}(\tau)$ gives directly, through (2.2) and (2.6), an experimental estimate of the mean-square particle displacement $\langle \Delta x^2(\tau)\rangle$.

2.2. The velocity autocorrelation function and mean-square displacement

Prior to the discovery of long-time tails the dynamics of Brownian motion were traditionally described by the simple Langevin equation (e.g. Uhlenbeck and Ornstein 1930, reprinted in Wax 1954)

$$m\dot{v}(t) = -fv(t) + F(t) \tag{2.7}$$

where m is the particle mass and $F(t)$ is the 'random force'. The frictional coefficient f is given by the Stokes expression

$$f = 6\pi\eta R \tag{2.8}$$

where η is the shear viscosity of the suspending fluid and R the particle radius. With the usual assumption that $F(t)$ is δ correlated it is straightforward to show that the velocity autocorrelation function $\phi(t)$ corresponding to equation (2.7) is

$$\phi(t) \equiv \langle v(0)v(t)\rangle = (kT/m) \exp[-(f/m)t] \tag{2.9}$$

where k is Boltzmann's constant and T the absolute temperature. The Einstein

expression for the particle diffusion constant D follows immediately from (2.9):

$$D \equiv \int_0^\infty \phi(t)\,\mathrm{d}t = kT/f. \tag{2.10}$$

Soon after their discovery it was recognised that long-time tails could be attributed physically to the effect on the particle of time-dependent velocity fields set up in the fluid by the particle motion itself. Mathematically this can be described by the addition of inertial and memory terms to equation (2.7) (Zwanzig and Bixon 1970, Widom 1971):

$$m\dot{v}(t) = -fv(t) - \tfrac{2}{3}\pi\rho R^3\dot{v}(t) - 6R^2(\pi\eta\rho)^{1/2}\int_{-\infty}^{t}\frac{\dot{v}(t')}{(t-t')^{1/2}}\,\mathrm{d}t' + F(t) \tag{2.11}$$

where ρ is the fluid density.

The determination of $\phi(t)$ from (2.11) has been discussed by many authors (see e.g. Pomeau and Résibois 1975, Zwanzig and Bixon 1975, Pusey 1979 for references, also Hinch 1975, Warner 1979, Jones 1980 for more recent work) and is best approached by Laplace transformation. The relevant mathematics are summarised in the appendix. The results needed here are given below.

(i) Equation (2.10) is still valid so that the long-time diffusion constant is not affected by the extra terms in (2.11).

(ii) The asymptotic behaviour of $\phi(t)$ at long times is given by

$$\lim_{t\to\infty}\phi(t) = \frac{D}{2\sqrt{\pi}}\left[T_L^{1/2}t^{-3/2} - \tfrac{1}{6}(7-4\rho_P/\rho)T_L^{3/2}t^{-5/2} + \ldots\right] \tag{2.12}$$

where ρ_P is the particle density and

$$T_L \equiv \rho R^2/\eta \tag{2.13}$$

is the characteristic time taken by a viscous shear wave to propagate across the particle (e.g. Landau and Lifshitz 1966, p 89).

(iii) The asymptotic behaviour of the mean-square displacement is

$$\begin{aligned}\langle\Delta x^2(\tau)\rangle &\equiv 2\int_0^\tau(\tau-t)\phi(t)\,\mathrm{d}t \\ &= 2D\left[\tau - \frac{2}{\sqrt{\pi}}T_L^{1/2}\tau^{1/2} + \frac{T_L}{9}\left(8-\frac{2\rho_P}{\rho}\right) - \frac{1}{9\sqrt{\pi}}\left(7-\frac{4\rho_P}{\rho}\right)T_L^{3/2}\tau^{-1/2} + \ldots\right].\end{aligned} \tag{2.14}$$

Thus, at large enough τ, $\langle\Delta x^2(\tau)\rangle$ reduces to the usual macroscopic expression

$$\lim_{\tau\to\infty}\langle\Delta x^2(\tau)\rangle = 2D\tau. \tag{2.15}$$

(iv) A useful quantity, which will be used in the data analysis (§ 4), is the 'time-dependent diffusion coefficient' defined by

$$D(\tau) \equiv \int_0^\tau \phi(t)\,\mathrm{d}t. \tag{2.16}$$

$D(\tau)$ is the local slope (at $t=\tau$) of a plot of $\langle\Delta x^2(t)\rangle/2$ against t and is given by

$$D(\tau) = D\left[1 - \frac{1}{\sqrt{\pi}}\left(\frac{T_L}{\tau}\right)^{1/2} + \frac{1}{18\sqrt{\pi}}\left(7-\frac{4\rho_P}{\rho}\right)\left(\frac{T_L}{\tau}\right)^{3/2} + \ldots\right]. \tag{2.17}$$

2.3. Detectability of the long-time tail

It is clear from equations (2.12)–(2.17) that the effect of the *long-time* tail in $\phi(t)$ on the quantities $\langle \Delta x^2(\tau) \rangle$ and $D(\tau)$ measured by light scattering is most marked at *short times* (and becomes negligible for $\tau/T_L \gg 1$). However, in such experiments an effective lower bound on the delay time τ is imposed by considerations of statistical accuracy. Photon correlation spectroscopy provides samples of $g^{(1)}(K, \tau)$ (equation (2.6)) at discrete times $\tau = pT_S$ ($p = 1, 2, \ldots, 88$, in our experiments) where T_S is a variable sample time, pre-set for a given experiment. As T_S is decreased, the decay of $g^{(1)}(K, \tau)$ from point to point becomes smaller whereas the statistical uncertainty in a given point generally becomes larger. Therefore the accuracy with which the decay of $g^{(1)}(K, \tau)$ and hence $D(\tau)$ can be measured also decreases. In the absence of long-time tail effects, the characteristic decay time of $g^{(1)}(K, \tau)$ is given by (equations (2.6) and (2.15))

$$T_C = (DK^2)^{-1}. \tag{2.18}$$

A measure of the detectability of long-time tail effects in light scattering measurements is therefore the ratio of the two times T_L (2.13) and T_C (see also Bouiller *et al* 1978):

$$T_L/T_C = (kT/6\pi)(\rho R/\eta^2)K^2. \tag{2.19}$$

It is evident that measurements should be made on large spheres in a high-density, low-viscosity fluid using as large a scattering vector as possible, i.e. with λ_0 small and θ large (equation (2.4)).

For our experiments ($D \approx 1.1 \times 10^{-9}$ cm^2 s^{-1}, $K^2 \approx 9.9 \times 10^{10}$ cm^{-2}, $R \approx 1.7$ μm, $\rho \approx 1.05$ g cm^{-3}, $\eta \approx 0.011$ poise), $T_C \approx 9.2 \times 10^{-3}$ s, $T_L \approx 2.8 \times 10^{-6}$ s so that $T_L/T_C \approx 3 \times 10^{-4}$. For the experiments of Bouiller *et al*, typically $T_C = 1.9 \times 10^{-4}$ s, $T_L = 1.1 \times 10^{-8}$ s and $T_L/T_C \approx 6 \times 10^{-5}$.

3. Experimental details

3.1. Sample characterisation and preparation

The large polystyrene spheres were prepared by Professor R H Ottewill and colleagues at Bristol University. The particle size was determined by Mie scattering. The data points in figure 1 show a measurement of the angular dependence of the average intensity of vertically polarised light ($\lambda_0 = 4762$ Å) scattered by a sample of the spheres suspended in water in a cell of square 1 cm × 1 cm cross section. The full curves in figure 1 are theoretical Mie scattering curves (e.g. Kerker 1969) adjusted by an arbitrary amplitude factor to fit the maxima in the data around $\theta = 90°$. The parameters m and α used in these calculations are indicated in the figure: m is the refractive index of the particles relative to that of the liquid and

$$\alpha = 2\pi Rn/\lambda_0. \tag{3.1}$$

The most noticeable difference between experiment and theory in figure 1 concerns the depths of the minima. The smaller experimental depths are almost certainly caused by multiple scattering which adds a background light level showing less angular structure than the single-scattered light. (The particular sample used, which was only intended for a rough measurement, transmitted only about 36% of the incident intensity.) Two features of the theoretical curves were found to be particularly sensitive to variations in α and m: the depth of modulation around $\theta = 50°$ and the 'shoulder' at $\theta \approx 98°$. After

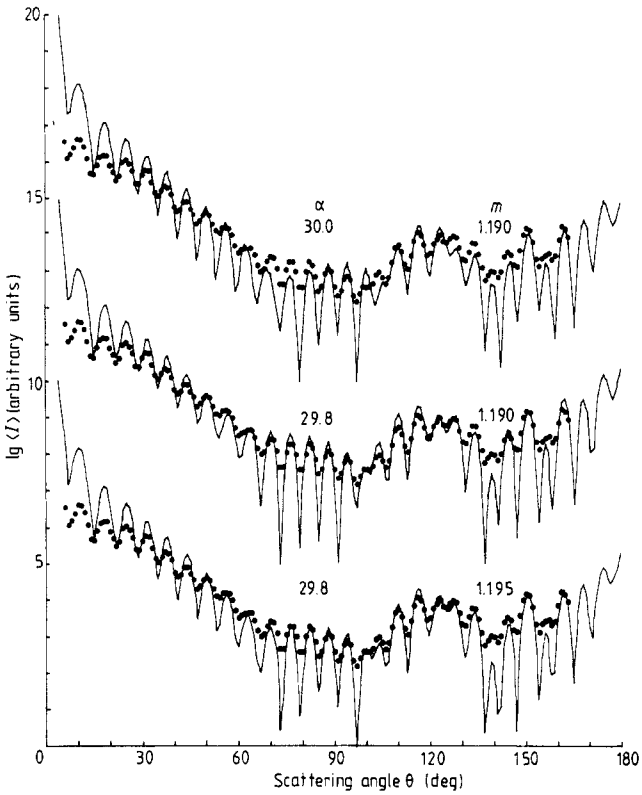

Figure 1. Particle sizing from Mie scattering profile. Logarithm of average intensity $\langle I \rangle$ is plotted against scattering angle θ. The same set of data (points) is compared with three theoretical profiles (continuous lines, α is size parameter (3.1), m is relative refractive index), displaced vertically for ease of presentation. Middle curve is judged to give best fit.

generating many theoretical curves for different α and m, we judged visually that the central curve in figure 1 fits the data best and therefore take $\alpha = 29.8 \pm 0.3$ and $m = 1.19 \pm 0.05$. Use of (3.1) with $n = 1.339$ then gives, for the particle radius, $R = 1.69 \pm 0.017$ μm.

We also tried averaging together theoretical curves over a range of α values to assess possible effects of polydispersity (a distribution of particle size). None of these, admittedly crude, attempts led to a better agreement with the experimental points. We conclude that the particles are virtually monodisperse with a standard deviation in particle size certainly less than 3% of the mean.

The samples used for photon correlation spectroscopy were prepared as follows: the concentrated stock suspension was shaken and allowed to settle for a few hours so that a boundary existed between clear water and the remaining suspension. A drop of suspension was withdrawn from just below the boundary in the hope that any aggregates or other impurities would have settled out of this region faster than the particles of interest. This drop of suspension was added to the sample cell which contained a well filtered (0.22 μm, Millipore) mixture of light and heavy water (or, in one case, just H_2O, § 5.4). The cell was shaken and excess suspension expelled by filtered air so that the final column of fluid was less than 1 cm high. The quartz sample cell had external cross sectional dimensions of 1.2×1.2 cm^2 and internal dimensions of 1×0.2 cm^2.

When the scattered laser light was observed by eye, samples prepared in this way appeared quite clean. Occasionally a scintillating speck ('dust') was observed, particularly at angles corresponding to minima in the Mie pattern (where the genuine scattering was weak). One sample was used for about a week and appeared slightly dirtier at the end of this time. Nevertheless we estimate that the intensity of the light scattered by dust was less than 1% of that scattered by the particles: no time-dependent degradation of photon correlation results was observed.

Particle number densities were estimated by using one of the simpler results of Mie scattering theory, namely that large enough particles have a total light-scattering cross section equal to twice their physical cross section πR^2 (e.g. Kerker 1969, p 104). For such particles it is straightforward to show that the fraction of incident light transmitted by a column of suspension of length l is $\exp(-l/L)$ where the attenuation length L is

$$L = (2\pi R^2 N)^{-1} \tag{3.2}$$

and N is the number of particles per unit volume. The samples used in this work had attenuation lengths in the range 2–3 cm corresponding to $N = 2.7 \times 10^6$–1.9×10^6 cm^{-3}. Thus a scattering volume of 10^{-3} cm^3 (§ 3.2) contains 2–3×10^3 particles.

3.2. Optics

Figure 2 shows the optical arrangement for the experiment. The light source was either a Spectra Physics model 164 Ar^+ ion laser or a Coherent model 500 K Kr^+ ion laser. The output power was typically 50–100 mW, stabilised by built-in feedback loops.

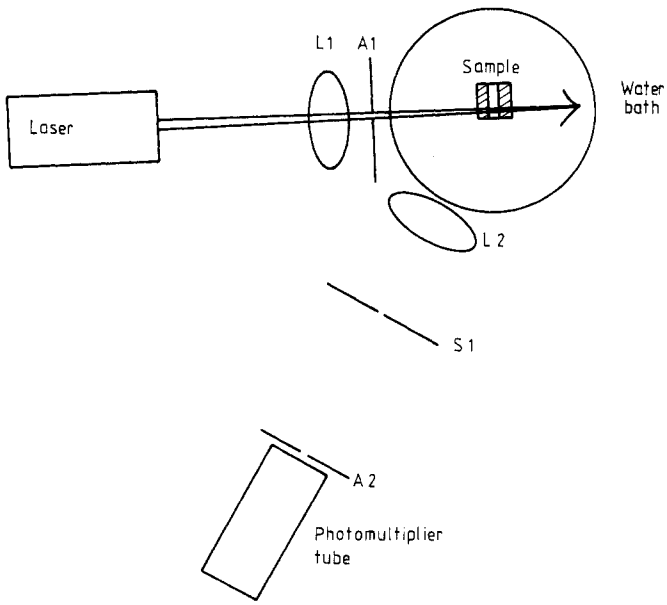

Figure 2. Plan view of optical arrangement. Laser beam is weakly focused by lens L1 through aperture A1 into sample contained in water bath. Lens L2 images sample cell onto vertical slit S1. Scattered light is collected by photomultiplier tube through 'coherence' aperture A2.

Intracavity circular apertures prevented the operation of transverse cavity modes so that spatial coherence of the output beam was assured. The laser beam was weakly focused (to obtain the necessary light intensity in the sample) with a lens L1 of focal length about 35 cm. The sample cell was placed with its short internal dimension (0.2 cm) parallel to the beam at a point about 8 cm from the beam focus where the beam diameter was about 0.1 cm. The cell was surrounded by a blackened aluminium block with slots to allow the entrance and exit of the light. The cell/block combination was immersed in a lagged cylindrical water bath of diameter about 15 cm and capacity about 3 l. Room temperature was controlled to 19.5 ± 0.3 °C, but the water temperature was not controlled separately. Typically the latter varied at a rate less than 0.05 °C h^{-1}. We felt this arrangement (small sample cell, aluminium block, large water bath) would be effective in minimising temperature gradients across the cell which could lead to convection.

The detection optics were mounted on a massive optical bench able to rotate about the axis of the water bath. The region of sample illuminated by the laser was imaged 1 : 1 by lens L2 onto a vertical slit of width 0.1 cm which served to discriminate against light scattered by the cell walls. The volume of sample 'seen' by the detector was thus about 10^{-3} cm^3, defined by the slit and the beam profile. The sample cell was mounted so that it could be moved in three orthogonal directions relative to the bath. After each change of scattering angle the cell was moved up and down the laser beam while the detected intensity was monitored. This allowed the image of the cell to be centred on the slit. The cell was always placed so that the illuminating beam was close to the exit (side) window of the scattered light (see figure 2). With this arrangement it was possible to make reliable measurements for scattering angles in the range $60 \leqslant \theta \leqslant 120°$. The actual value of θ was always chosen to coincide with a maximum in the Mie scattering profile, thus ensuring high single-scattered intensity and discriminating against dust and multiple scattering (see § 6.7). Uncertainty in the scattering angle was estimated as $\pm 0.2°$.

3.3. Electronics and data analysis

The detector was an ITT FW130 photomultiplier tube operated in the photon-counting mode. It was preceded by a circular aperture of diameter 200 μm placed about 60 cm behind the slit. The scattered light was nearly coherent across this aperture so that the constant c (§ 2.1) always had a value of about 0.8 or above (see e.g. figure 3).

The standardised photomultiplier signal was fed to a Malvern 'one-bit' digital correlator operated in the single-scaled mode. The correlator had 88 channels corresponding to delay times $\tau = pT_S$ ($p = 1$ to 88, T_S is the sample time) and four channels at delay times $345T_S$ to $348T_S$. The correlator was interfaced to a Hewlett–Packard 9830 computer which could be used to control a sequence of experiments as well as for data analysis. Data were usually accumulated in the form of many experiments of typical duration 10^3 s. The data for each 10^3 s experiment were normalised by the 'accidental' correlation rate ($\langle I \rangle^2$ in equation (2.1)) calculated from the total numbers of sample times, scaled counts and unscaled counts accumulated in separate monitor channels. (A check of the validity of this procedure is described in § 6.1.) Normalised data sets, $g^{(2)} - 1$, could then be averaged to give an effective experimental duration of as long as 28 h (table 1).

Photon counting rates were kept around 10^5 s^{-1}, low enough that dead-time effects are small but large enough for reasonable counting statistics.

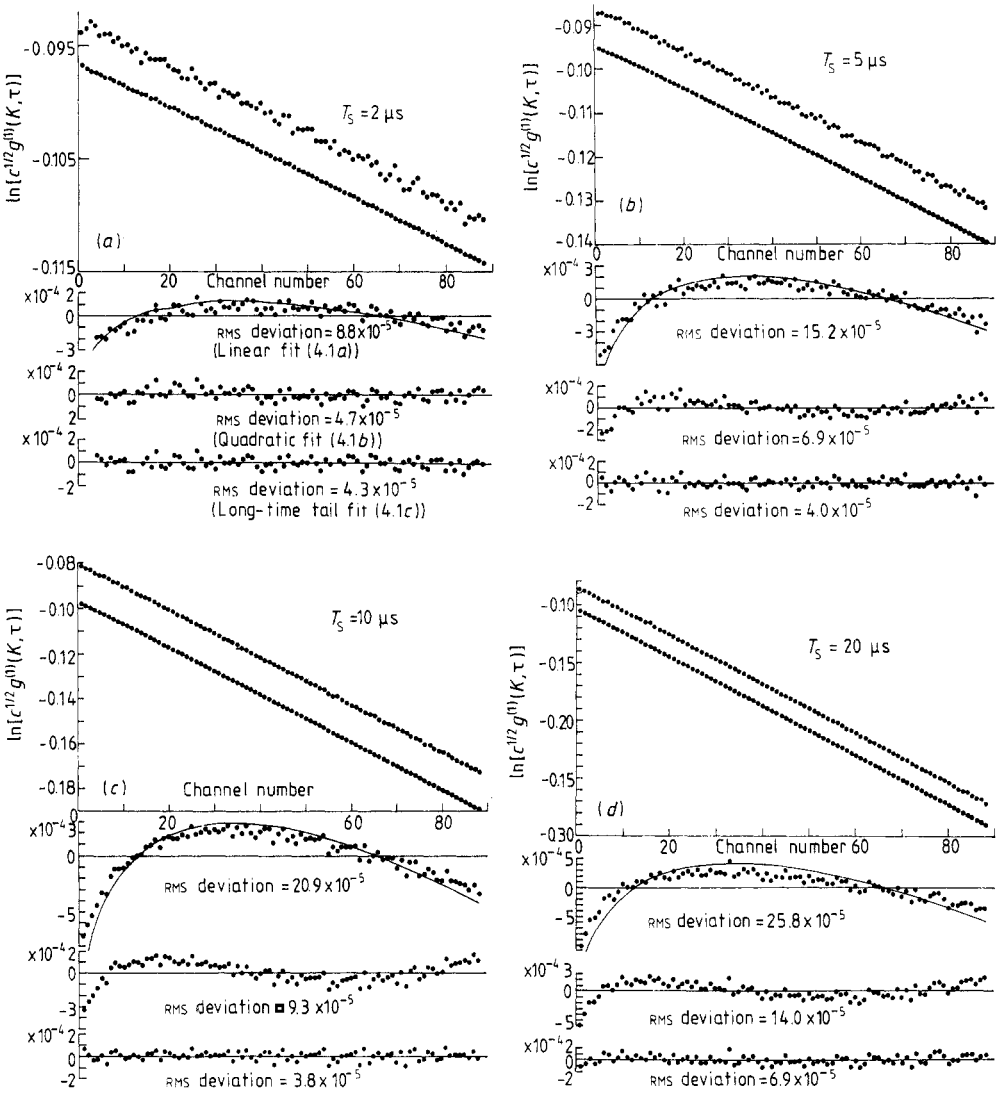

Figure 3. Log correlation functions, $\ln[c^{1/2}g^{(1)}(K,\tau)]$, showing marked long-time tail effects (§ 4) for four different sample times T_S (as indicated). Uppermost curve (displaced vertically) in each figure is from a single experiment of duration 10^3 s. Second curve is result of averaging many such experiments (see text). Bottom three curves are residuals (data point − fitted function) for the fit to theoretical linear, quadratic and 'long-time tail' expressions (4.1*a*)–(4.1*c*). The root mean square deviations *per point* are also shown for these fits. In all cases the long-time tail expression (bottom curve) fits best. The full curves in the top residual plots are equation (4.3), the theoretical prediction for the force fit of data showing long-time tail effects to a linear function.

From equations (2.2) and (2.6) we see that a measurement of $g^{(2)}-1$ provides an experimental estimate of $c(g^{(1)})^2$ and that

$$\tfrac{1}{2}\ln(g^{(2)}-1)=\tfrac{1}{2}\ln c+\ln g^{(1)}=\tfrac{1}{2}\ln c-\tfrac{1}{2}K^2\langle\Delta x^2(\tau)\rangle. \tag{3.3}$$

In the data analysis $\frac{1}{2}\ln(g^{(2)}-1)$ was fitted by linear least-squares programs to various

Table 1. Data analysis for figure 3.

Sample time T_S (μs)	$88T_S/T_C$	Number of experiments	Coefficients of fits (4.1a)–(4.1c); standard deviations in parentheses: Linear (4.1a) a (cm^2 s^{-1})	Quadratic a (cm^2 s^{-1})	(4.1b) b (cm^2 s^{-2})	Long-time tail (4.1c) a (cm^2 s^{-1})	d (cm^2 s$^{-1/2}$)
2	0.019	83×10^3 s (23.1 h)	1.010×10^{-9} (0.002)	0.946×10^{-9} (0.005)	-34.9×10^{-8} (2.6)	1.107×10^{-9} (0.006)	1.69×10^{-12} (0.11)
5	0.048	103×10^3 s (28.6 h)	1.037×10^{-9} (0.001)	0.996×10^{-9} (0.002)	-9.55×10^{-8} (0.56)	1.098×10^{-9} (0.002)	1.58×10^{-12} (0.05)
10	0.097	46×10^3 s (12.8 h)	1.061×10^{-9} (0.001)	1.031×10^{-9} (0.002)	-3.38×10^{-8} (0.2)	1.104×10^{-9} (0.002)	1.57×10^{-12} (0.03)
20	0.194	27×10^3 s (7.5 h)	1.073×10^{-9} (0.001)	1.056×10^{-9} (0.001)	-1.02×10^{-8} (0.07)	1.100×10^{-9} (0.002)	1.36×10^{-12} (0.04)

trial functions which included both theoretical models for $\langle\Delta x^2(\tau)\rangle$ and functions which allowed for some of the more common systematic errors (see §§ 4 and 6). In these analyses the data points were weighted according to the procedure of Pusey *et al* (1974). Two approaches were taken to the data analysis: firstly data from the individual 10^3 s experiments were fitted to the trial functions and the coefficients obtained from many such experiments were averaged to give their mens and standard deviations. Secondly the data sets were averaged first, as outlined above, and the result was then analysed. The mean values of the coefficients obtained by these two procedures agreed very well in all cases. However the estimated standard deviations differed occasionally by as much as a factor of two. In §§ 4 and 5 the values of standard deviation quoted are the larger of the values obtained in the two analysis procedures.

4. Results showing marked long-time tail effects

The largest amount of experimental data was obtained from a sample of number density $N\approx2.7\times10^6$ cm^{-3} (§ 3.1) in a D_2O/H_2O mixture at scattering angle $\theta=118°$, with sampling times $T_S=2$, 5, 10 and 20 μs (much smaller than T_C, § 2.3) and the $\lambda_0=4579$ Å argon laser line. It is under these conditions of short sampling times and large scattering vector that long-time tail effects should be most visible (§ 2.3).

In figures 3(a)–(d) logarithms of the measured field correlation functions, $\frac{1}{2}\ln(g^{(2)}-1)$, are plotted as a function of delay time for the four sample times. The uppermost traces in each figure are for a typical single 10^3 s experiment whereas the lower traces show the results of averaging the number of experiments listed in table 1. With a counting rate of 10^5 s^{-1} the average photon number $\langle n\rangle$ per sample time is, for $T_S=10$ μ s, about one. This is the optimum condition for good counting statistics and these are evident in figures 3(c) and 3(d). For $T_S=5$ and 2 μs, $\langle n\rangle<1$ and more statistical error is evident in figures 3(a) and 3(b), exacerbated by the smaller vertical differences between points (note the different vertical scales in figures 3(a)–(d)).

In all cases the log correlation functions show a downward curvature although this is not a striking effect when the data are presented in this form. Accordingly we also show in figures 3 the residuals (data point − fitted function) for the fit to three trial functions

(see equations (3.3), (2.14) and (2.15)):

$$\text{linear} \qquad \ln c^{1/2} - K^2 a\tau \tag{4.1a}$$

$$\text{quadratic} \qquad \ln c^{1/2} - K^2(a\tau - b\tau^2) \tag{4.1b}$$

$$\text{'long-time tail'} \qquad \ln c^{1/2} - K^2(a\tau - d\tau^{1/2}). \tag{4.1c}$$

The quadratic expression is chosen since a number of experimental artefacts are expected to result in functions of this form (§ 6). When fitting the $T_S = 2\ \mu$s data the first three points were omitted since they appear to show systematic deviations probably associated with photomultiplier tube afterpulsing (§ 6.1). Also given in figures 3(*a*)–(*d*) are the RMS deviations (per point) between data and fit, a criterion of 'goodness of fit'. It is immediately apparent (especially in figures 3(*b*)–(*d*), where statistics are reasonably good) that only the 'long-time tail' function gives an adequate fit of the data when judged in terms of both lack of structure in the plots of residuals and the RMS deviations.

In table 1 we list the coefficients a, b and d, along with their standard deviations (§ 3.3), obtained from the fits. The validity of fit (4.1*c*) is confirmed by the fact that only in this case are the coefficients obtained more or less independent of the sample time T_S used.

Two other types of fit were also tried:

$$\text{'second-order long-time tail'} \qquad \ln c^{1/2} - K^2(a\tau - d\tau^{1/2} - e\tau^{-1/2}) \tag{4.1d}$$

$$\text{long-time tail and quadratic} \qquad \ln c^{1/2} - K^2(a\tau - b\tau^2 - d\tau^{1/2}). \tag{4.1e}$$

For $T_S = 2$, 5 and 10 μs neither (4.1*d*) nor (4.1*e*) gave a significantly better fit than (4.1*c*). However for $T_S = 20\ \mu$s, both (4.1*d*) and (4.1*e*) showed significant improvements. It is unlikely that the $\tau^{-1/2}$ term in (4.1*d*) will be important at $T_S = 20\ \mu$s if it is not detectable at smaller T_S. However a τ^2 term, evident at larger T_S, can, as mentioned previously, be caused by various experimental artefacts (§ 6). For $T_S = 20\ \mu$s fit (4.1*e*) gives a coefficient $d = 1.70 \pm 0.1 \times 10^{-12}$ cm^2 s$^{-1/2}$ which brings it into line with the values obtained at shorter sample times (table 1).

The values obtained for the coefficients a and d can be compared with the theory (§ 2.2). The coefficient a should simply be D, the long-time diffusion coefficient of the particle (equations (2.6) and (2.14)). Unfortunately, due to uncertainties in the sample preparation, the composition of the D_2O/H_2O mixture was not known exactly though we believe it to be about 40% D_2O by volume. Without incurring significant error we take the refractive index of the mixture to be $n = 1.339$, that of pure water at $\lambda_0 = 4579$ Å. This gives $K^2 = 9.92 \times 10^{10}$ cm^{-2} (equation (2.4)) at $\theta = 118°$, a result which has already been used when calculating the coefficients quoted in table 1. We assume that the density ρ and viscosity η of the mixture are linear combinations of those of its constituents. Taking $\rho_{D_2O} = 1.105$ g cm^{-3} and $\eta_{D_2O} \approx 1.23$ cp at 19.5 °C (Smithsonian Physical Tables 1964, p 320) we get $\rho = 1.042$ g cm^{-3} and $\eta = 1.10$ cp. Averaging the data for $T = 2$, 5 and 10 μs (where (4.1*c*) gives the best fit) gives $D = 1.101 \pm 0.004 \times 10^{-9}$ cm^2 s^{-1} so that, from equations (2.8) and (2.10), the apparent particle radius is $R = 1.770 \pm 0.006\ \mu$m. This is to be compared with $R = 1.69 \pm 0.017\ \mu$m obtained from the Mie scattering profile (§ 3.1). The error quoted for the light scattering radius is just the run-to-run statistical error. Systematic error associated with uncertainty in the composition of the D_2O/H_2O mixture could be as

much as 2%. Thus the difference between the radii values determined by these two methods is about 4.5%, roughly twice their estimated combined error (see below).

The theoretical expression for the coefficient d is (equations (2.6), (2.13), (2.14) and (4.1c))

$$d_{\text{th}} = kT\rho^{1/2}/3(\pi\eta)^{3/2} \tag{4.2}$$

so that for T, ρ and η as given above, $d_{\text{th}} = 2.14 \times 10^{-12}\ \text{cm}^2\ \text{s}^{-1/2}$. This is to be compared with the value $d = 1.58 \pm 0.05 \times 10^{-12}\ \text{cm}^2\ \text{s}^{-1/2}$ obtained by averaging the experimental results (weighted by the inverse of their variances) for $T_S = 2$, 5 and 10 μs. Thus the experimental value is only about $74 \pm 3\%$ of the theoretical value, and the difference between the two is many times the estimated statistical error in the measurement.

Possible sources of systematic error in this type of light scattering experiment are discussed in § 6. There are several effects (e.g. heterodyning, dust and dimerisation) which could lead to a reduction in the coefficient a and hence an apparent increase in R of the magnitude found above (~4.5%). However all of these are expected to give a similar reduction in the coefficient d of the $\tau^{1/2}$ term. The much greater reduction observed must therefore either be caused by some unconsidered systematic error or indicate a real failing of the theory outlined in § 2 (see § 7).

A more direct way of presenting the data is to perform a numerical differentiation of the curves shown in figures 3(a)–(d) to obtain the time-dependent diffusion coefficient $D(\tau)$ for direct comparison with equation (2.17). This is shown in figure 4. The differentiation was accomplished by taking sets of j consecutive data points and performing a least-squares fit of their logarithms to a linear function of τ. $D(\tau)$ was then

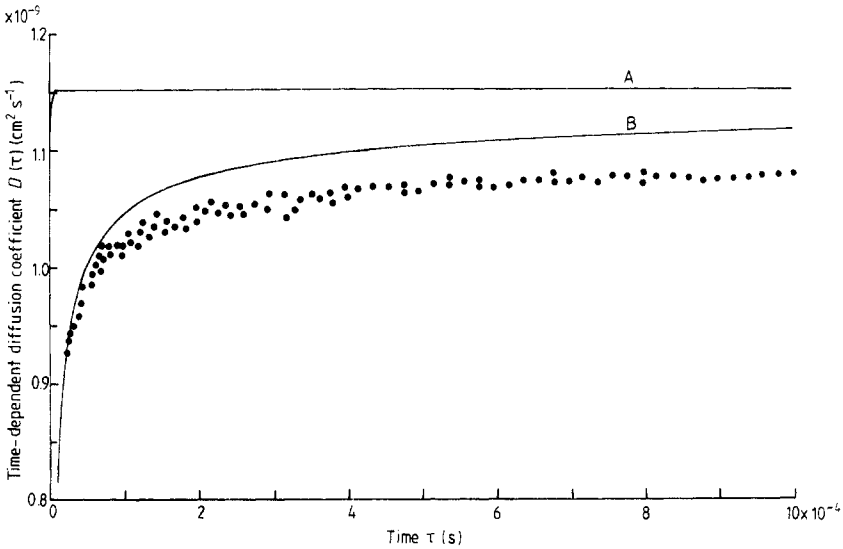

Figure 4. Data points are 'time-dependent diffusion coefficient' (2.16) obtained by numerical differentiation of data of figure 3. Full curve A is the theoretical prediction for an exponentially decaying (2.9) velocity autocorrelation function i.e. no long-time tail. Curve B is equation (2.17), the theoretical prediction incorporating long-time tail effects. While differences between experiment and theory are evident the data clearly support the existence of a long-time tail.

obtained from the slope of this line; τ was taken to be the delay time corresponding to the central point of the set. The optimum number j for each sample time was chosen visually to give the best compromise between statistical error for too small j and systematic error for too large j. The values of j used to obtain figure 4 were 20 for $T_S = 2\ \mu$s, 14 for $T_S = 5\ \mu$s, and 10 for $T_S = 10$ and 20 μs.

The data in figure 4 are compared with two theoretical cruves A and B taking $R = 1.69\ \mu$m and other parameters as given above. Curve A is (2.16) with the exponentially decaying velocity autocorrelation function (2.9); this curve clearly does not fit the data which therefore implies a much slower decay in $\phi(t)$. Curve B is the first two terms of the theoretical 'long-time tail' prediction (2.17). The data follow the general shape of this curve though the differences mentioned above between experiment and theory are evident. It should be emphasised that (if the radius determined by Mie scattering is taken to be correct) there are *no* adjustable parameters in this latter comparison. (At first sight it appears from figure 4 that there is agreement between experiment and theory for $\tau \leqslant 5 \times 10^{-5}$ s; however, in terms of the least-squares analysis given above, a more likely explanation of this apparent agreement is an 'accidental' cancellation of the effects of the differences between the theoretical and experimental values of d and D for this particular range of τ.) Addition of the third term in (2.17) to curve B made a barely detectable difference, thus confirming its undetectability in our measurements.

Finally we note that the (unweighted) least-squares fit of a function of the form of (4.1c) to a straight line can be performed analytically (in integral rather than summation form) with the result

$$\text{Residual} = K^2 d[\tau^{1/2} - \tfrac{4}{15}T_T^{1/2} - \tfrac{4}{5}(\tau/T_T^{1/2})] \tag{4.3}$$

where $T_T \equiv 88T_S$ is the total delay time spanned by the 88 correlator channels. Equation (4.3), with the theoretical value of d (4.2), is plotted as the full curves in figure 3. As expected from the discussion above, the data residuals show the same general form as (4.3) indicating the presence of a $\tau^{1/2}$ term in $\langle \Delta x^2(\tau) \rangle$. However their magnitudes are clearly only about 75% of the predicted values (see figure 3(c) in particular).

5. Supplementary data

5.1. Introduction

Although the data presented in § 4 are more or less consistent within themselves it is important to check the overall validity of our approach by making further measurements under a range of experimental conditions. The supplementary data reported in this section include measurements made at longer delay times, at smaller scattering vectors and a few experiments on particles suspended in 100% H_2O.

5.2. Long delay time, D_2O/H_2O mixture, $\theta = 118°$ and $\lambda_0 = 4579$ Å

First we discuss measurements made on the same sample as those reported in § 4 under the same experimental conditions except only that the correlator sample time T_S was 300 μs. Thus the total time spanned by 88 channels was about $3T_C$. Thirty seven experiments of 600 s duration were performed. Figure 5 shows semilogarithmic plots

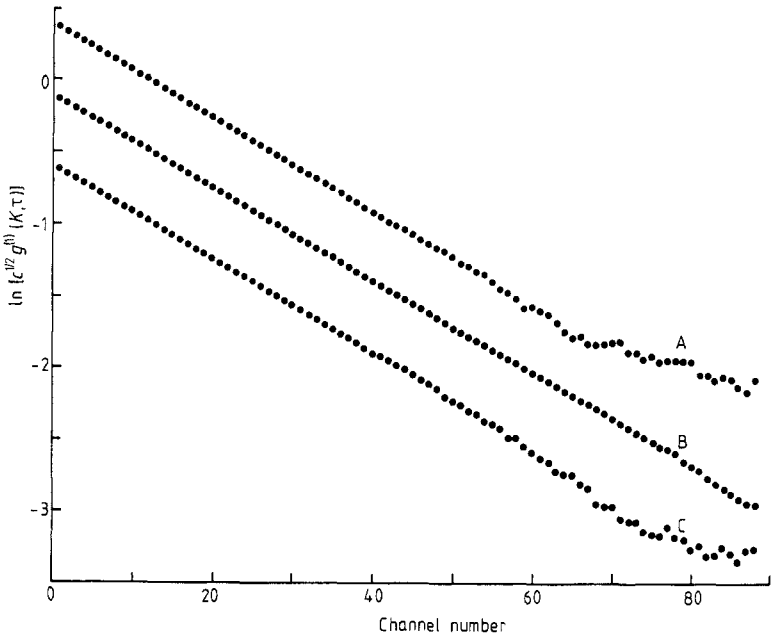

Figure 5. Data obtained under same conditions as for figure 3 *except* at much longer sample time $T_S = 300$ μs (§ 5.2). Curves A and C (displaced vertically) are for single experiments of duration 600 s. Curve B is the average of 37 such experiments.

of two typical individual experiments (curves A and C) and of the average of all 37 experiments (curve B). The results of fitting this average to the trial functions of equations (4.1*a*)–(4.1*c*) and (4.1*e*) are given in table 2. Here we also quote the familiar normalised second cumulant Q,

$$Q \equiv 2b/K^2a^2, \tag{5.1}$$

which is twice the coefficient of the τ^2 term in $\ln g^{(1)}$ divided by the square of the coefficient of τ (Pusey *et al* 1974).

The positive second cumulant Q and negative value for d in fits (4.1*b*) and (4.1*c*) indicate an overall upward curvature in $\ln g^{(1)}$ though this is barely significant. Fit (4.1*e*) gives a value of D in good agreement with that obtained at shorter times (§ 4); also the value of d obtained in this fit is not inconsistent with that obtained previously though the statistical error is much larger.

Table 2. Data analysis for figure 5, $T_S = 300$ μs, $88T_S/T_C \approx 2.9$, 37×10^3 s experiments (10.3 h

Coefficients of fits (4.1*a*)–(4.1*c*) and (4.1*e*)							
Linear (24*a*)	Quadratic (4.1*b*)		Long-time tail (4.1*c*)		Long-time tail + quadratic (4.1*e*)		
a (cm^2 s^{-1})	a (cm^2 s^{-1})	$Q \equiv 2b/K^2a^2$	a (cm^2 s^{-1})	d (cm^2 s$^{-1/2}$)	a (cm^2 s^{-1})	Q	d (cm^2 s$^{-1/2}$)
1.089×10^{-9}	1.094×10^{-9}	0.01	1.084×10^{-9}	-0.6×10^{-12}	1.113×10^{-9}	0.019	1.40×10^{-12}
(0.002)	(0.004)	(0.007)	(0.023)	(1.1)	(0.03)	(0.03)	(1.70)

The averaged correlation function in the last four delayed channels (§ 3.3) was 1.0007 ± 0.0003, to be compared with the theoretical value of essentially 1.0000. This indicates a small unimportant effect due probably to a changing mean count rate associated with number fluctuations (§ 6.4).

Thus these long-delay-time data are almost completely consistent with the data described in § 4 and give no indication of serious systematic error which could affect the latter measurements.

5.3. Smaller angle, $\theta = 66°$, D_2O/H_2O mixture, $\lambda_0 = 4579$ Å

A few measurements were made on the same sample as that used hitherto but at scattering angle $\theta = 66°$ (where $K^2 = 4.006 \times 10^{10}$ cm^{-2} as opposed to 9.921×10^{10} cm^{-2} at $\theta = 118°$). The results of the analysis of these data are given in table 3. At short sample times $T_S = 5$ and 10 μs it was again found that equation (4.1*c*) gave the best fit. The value of D obtained in this way was about 1.9% greater than that found at $\theta = 118°$. This difference is within the expected combined systematic error composed of temperature and angle uncertainty (§ 3.2) and back reflections from the cell walls (§ 6.5). The coefficient d of the $\tau^{1/2}$ term shows (as expected, § 2.3) a larger statistical error than at $\theta = 118°$ but is otherwise in excellent agreement with the large-angle value.

The semilogarithmic plot of the average of the correlation functions obtained at large sample time $T_S = 700$ μs showed a small but distinct upward curvature described by the positive second cumulant Q in the quadratic fit. The reasons for this long-time non-linearity were not determined unambiguously but probably include a combination of the effects described in § 6.

Table 3. Data analysis for § 5.3.

Sample time T_S (μs)	$\frac{88T_S}{T_C}$	Number of experiments	Coefficients of fits (4.1*a*)–(4.1*c*)				
			Linear (4.1*a*)	Quadratic (4.1*b*)		Long-time tail (4.1*c*)	
			a (cm^2 s^{-1})	a (cm^2 s^{-1})	Q	a (cm^2 s^{-1})	d (cm^2 s$^{-1/2}$)
5	0.019	41×10^3 s (11.4 h)	1.065×10^{-9} (0.003)	1.021×10^{-9} (0.004)	−4.67 (0.40)	1.125×10^{-9} (0.004)	1.60×10^{-12} (0.11)
10	0.039	18×10^3 s (5 h)	1.075×10^{-9} (0.004)	1.045×10^{-9} (0.003)	−1.53 (0.02)	1.118×10^{-9} (0.005)	1.62×10^{-12} (0.12)
700	2.7	26×700 s (5.1 h)	1.059×10^{-9} (0.007)	1.085×10^{-9} (0.01)	0.044 (0.01)	1.019×10^{-9} (0.03)	-7.3×10^{-12} (2)

Long-time tail + quadratic (4.1*e*)		
a (cm^2 s^{-1})	Q	d (cm^2 s$^{-1/2}$)
1.083×10^{-9} (0.04)	0.043 (0.030)	-0.22×10^{-12} (2.0)

5.4. Pure water, $\lambda_0 = 6471$ Å, $\theta = 116°$

Finally measurements were made on a slightly more dilute sample ($N \approx 1.9 \times 10^6$ cm^{-3}) of particles suspended in pure water using the 6471 Å line of the Kr^+ laser and a

scattering angle $\theta = 116°$. ($K^2 = 4.805 \times 10^{10}$ cm^{-2}). The data analysis and other experimental details are summarised in table 4. Two different laser intensities were used in these measurements providing counting rates of about 8×10^4 s^{-1} and 4×10^4 s^{-1}. It is evident that the fitted coefficients are all slightly lower at the lower counting rate though the difference is barely significant.

Table 4. Data analysis for § 5.4.

Sample time T_S (μ_s)	$88T_S/T_C$	Number of experiments — counting rate	Coefficients of fits: Linear a (cm^2 s^{-1})	Quadratic a (cm^2 s^{-1})	Quadratic Q	Long-time tail a (cm^2 s^{-1})	Long-time tail d (cm^2 s$^{-1/2}$)
10	0.047	12×10^3 s (3.3 h) / 8×10^4 s^{-1}	1.160×10^{-9} (0.003)	1.128×10^{-9} (0.003)	−1.185 (0.13)	1.205×10^{-9} (0.007)	1.69×10^{-12} (0.15)
10	0.047	13×2000 s (7.2 h) / 4×10^4 s^{-1}	1.144×10^{-9} (0.004)	1.113×10^{-9} (0.004)	−1.17 (0.14)	1.183×10^{-9} (0.005)	1.48×10^{-12} (0.19)

Sample time T_S (μ_s)	$88T_S/T_C$	Number of experiments — counting rate	Quadratic a	Quadratic Q	Long-time tail + quadratic a	Long-time tail + quadratic Q	Long-time tail + quadratic d
500	2.33	4×10^3 s (1.1 h) / 8×10^4 s^{-1}	1.175×10^{-9} (0.005)	0.058 (0.012)	1.187×10^{-9} (0.04)	0.063 (0.02)	1.35×10^{-12} (0.53)
500	2.33	4×10^3 s (1.1 h) / 4×10^4 s^{-1}	1.161 (0.005)	0.034 (0.017)	1.160×10^{-9} (0.04)	0.036 (0.03)	0.3×10^{-12} (1.0)

At short sample times $T_S = 10$ μs equation (4.1c) was again found to give the best fit. The particle radius obtained from the diffusion coefficient for these short-time measurements was $R = 1.77 \pm 0.02$ (equations (2.8) and (2.10), taking $T = 19.5$ °C and $\eta = 1.014$ cp). This is in excellent agreement with the value obtained in the D_2O/H_2O mixture and confirms our estimate of the composition of this latter mixture. The experimental value of d, the coefficient of the $\tau^{1/2}$ term in (4.1c), is $68 \pm 7\%$ of the value $d = 2.37 \times 10^{-12}$ cm^2 s$^{-1/2}$ predicted theoretically (equation (4.2)), just in agreement with the more precise measurements reported in § 4.

At longer sample times, $T_S = 500$ μs, an upward curvature was found in the semilogarithmic plots of the correlation functions as was the case for the data reported in § 5.3.

6. Possible sources of systematic error

6.1. Electronic distortions

Because the effects sought in this experiment are so small it is clearly important to evaluate any potential source of distortion. A simple but quite comprehensive check of the operation of the electronics (photomultiplier tube, pulse standardisation circuitry

and correlator system) can be made by illuminating the PMT with light of constant intensity. Then the normalised intensity correlation function $g^{(2)}(\tau)$ (equation (2.1)) should simply be 1 at all delay times. Figure 6 shows the results of several such measurements. The light source was an incandescent bulb powered by large batteries. When temporal and spatial averaging is accounted for, residual intensity fluctuations in the light are expected to be less than 1 part in 10^9; however undetermined systematic fluctuations could be larger. Measurements of duration about 12 h were made at a sample time $T_S = 5\ \mu s$ with three different counting rates $\sim 2.3 \times 10^5\ s^{-1}$, $\sim 1 \times 10^5\ s^{-1}$ and $\sim 4 \times 10^4\ s^{-1}$.

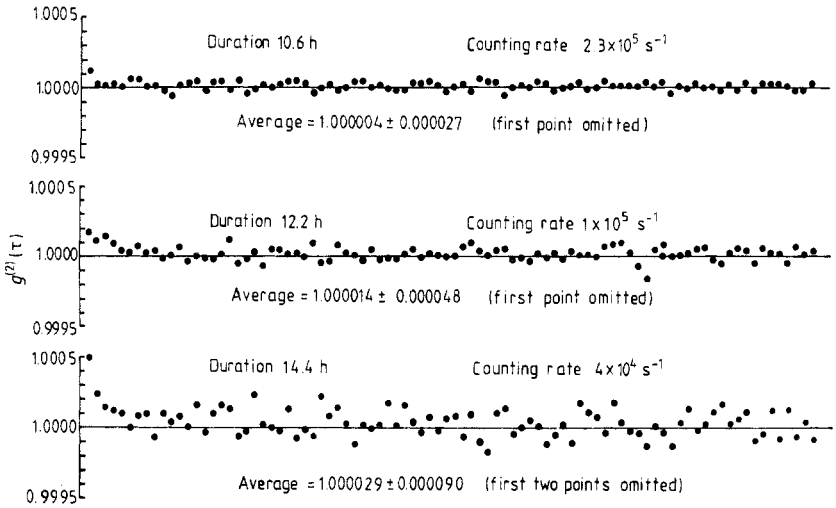

Figure 6. Intensity correlation functions $g^{(2)}(\tau)$ for white light. Sample time was $T_S = 5\ \mu s$. Experimental durations, counting rates, means and standard deviations (per point) are indicated.

Figure 6 shows that, except at short delay times, the correlation functions observed are essentially flat so that serious artefacts are not indicated. The means and standard deviations (per point) are given in figure 6. In all cases the means exceed the theoretical value of 1 by slightly more than the expected statistical error (the standard deviation per point/$\sqrt{88}$). However the difference is small. Potentially more serious are the spurious correlations, probably caused by photomultiplier tube 'afterpulsing' (e.g. Oliver 1974), evident in the first few channels. Such short-time distortions are apparent in the data of figure 3(*a*) and the first three points were omitted in the data analysis (§ 4). No distortions are obvious in figures 3(*b*)–(*d*) though, from figure 6, one might expect a small effect. Nevertheless we tried omitting the initial points when analysing these data and conclude that the effect of any electronic distortions on the fitted coefficients is comparable with their quoted statistical errors.

6.2. Residual flows in the sample

Some preliminary experiments were performed on samples contained in a large cell (internal dimensions 1 cm × 1 cm × ~2 cm high). We frequently found that the semi-logarithmic plots of the field correlation functions obtained with these samples showed

a marked downward curvature which was not reproducible in different experiments. A force fit of these plots to a straight line (equation (4.1*a*)) invariably gave an effective diffusion constant *greater* than that predicted by the Stokes–Einstein equation. We attribute this effect to residual flows in the sample caused, probably, by convection. Since genuine long-time tail effects also lead to downward curvatures in the semi-logarithmic plots it is important to understand artefacts due to residual flows.

It can be shown that any velocity gradient in the scattering plane caused by processes other than Brownian motion is problematic. For simplicity we assume that the particles in the scattering volume are divided into two equal groups which move relative to each other in the flow with a component Δv of velocity difference in the direction of the scattering vector $\boldsymbol{K}$. It is then straightforward to show that, in the presence of Brownian motion, this simple model leads to an effective field correlation function

$$c^{1/2}g^{(1)}(K,\tau) \equiv (g^{(2)}(K,\tau)-1)^{1/2}$$
$$= c^{1/2}\exp(-\tfrac{1}{2}K^2\langle\Delta x^2(\tau)\rangle)(\tfrac{1}{2}+\tfrac{1}{2}\cos K\Delta v\tau)^{1/2}$$

so that

$$\ln g^{(1)}(K,\tau) = -\tfrac{1}{2}K^2\langle\Delta x^2(\tau)\rangle - \tfrac{1}{8}(K\Delta v\tau)^2 + \ldots. \tag{6.1}$$

Thus residual flows in the sample introduce a *negative* τ^2-dependent term at small delay times (and hence the aforementioned downward curvature). In the absence of long-time tail effects we have

$$\ln g^{(1)}(K,\tau) = -DK^2\tau - \tfrac{1}{8}(K\Delta v\tau)^2 + \ldots \tag{6.2}$$

with an effective time-dependent diffusion coefficient (obtained by differentiation of (6.2)) given by

$$D(\tau) = D + \tfrac{1}{4}\Delta v^2\tau + \ldots. \tag{6.3}$$

In general the flow pattern will be more complex than that considered here. Nevertheless, provided that the local flow velocity leads to motion over a distance large compared with $2\pi K^{-1}$ ($\lesssim 0.5\ \mu$m) before its nature changes significantly, it can be shown that the functional form of equations (6.2) and (6.3) holds (Fuller *et al* 1980).

As discussed in § 4, the data shown in figures 3(*a*)–(*d*) are not described well by equation (6.2) (or equation (4.1*b*)). In addition the data for $D(\tau)$ presented in figure 4 do not show the linear increase with τ predicted by (6.3). We conclude, therefore, that our efforts to eliminate residual flows by using a small sample volume and large water bath (§ 3.2) were successful. This claim is supported by the observation of a fairly sharp horizontal boundary between dispersion and clear water as the particles sedimented.

6.3. Sedimentation

Even when residual flows have been eliminated there will, in general, be a coherent motion of the particles due to sedimentation. If this motion is strictly perpendicular to the scattering plane, extra fluctuations in the scattered intensity will be caused purely by the changing population of particles in the scattering volume. It can then be shown (Jakeman 1975) that, if the laser beam has a Gaussian profile, the effective field correlation function is

$$g^{(1)}(K,\tau) = \exp(-\tfrac{1}{2}K^2\langle\Delta x^2(\tau)\rangle)\exp[-\tfrac{1}{2}(\tau/T_{\text{sed}})^2] \tag{6.4}$$

so that, again, a negative τ^2-dependent term appears in $\ln g^{(1)}$. The characteristic time

T_{sed} is given by $T_{sed} = W_0/v_{sed}$ where W_0 is the radius of the laser beam at its focus and v_{sed} is the sedimentation velocity:

$$v_{sed} = 2R^2\Delta\rho g/9\eta \tag{6.5}$$

where the density difference $\Delta\rho = \rho_P - \rho$ and g is the acceleration due to gravity. For the optical arrangement of figure 1, $W_0 \approx 30\,\mu$m and, for polystyrene particles ($\rho_P \approx 1.055$ g cm^{-3}) of radius 1.77 μm suspended in water, $v_{sed} \approx 3.8\times10^{-5}$ cm s^{-1} (1 cm in about 7.5 h). Thus $T_{sed} \approx 80$ s and, even at $\tau = 7\times10^{-2}$s (the longest delay time used here), the effect of sedimentation is entirely negligible.

The decision to use a D_2O/H_2O mixture to reduce sedimentation was made prior to the above calculations which indicate a negligible effect. It was nevertheless advantageous in providing a sedimentation rate of less than 1 cm per day so that more frequent shaking of the sample to redisperse the particles was not necessary.

6.4. Heterodyning, number fluctuations and dust

In this subsection we consider three possible sources of error which, although different in nature and cause, can be treated in a single calculation. We take the measured intensity correlation function (normalised as described in § 3.3) to be of the form

$$g^{(2)}(K,\tau) = 1 + c(\exp(-2Y) + x\exp(-Y) + B) \tag{6.6}$$

where

$$Y = K^2(a\tau - d\tau^{1/2}) \tag{6.7}$$

(cf equation (4.1c)). The constants x and B are assumed to be small compared with unity. In the case of heterodyning some light scattered elastically by, for example, the cell walls is detected. This light can mix coherently with the genuine scattered light giving rise to the second term in brackets in (6.6); for pure heterodyning $B = 0$. If the number of particles in the scattering volume changes significantly (but slowly) during an experiment the result is the term B in (6.6), taken to be time-independent for slow enough variation. A fluctuating number of slowly moving dust particles contributes to both second and third terms in the brackets in (6.6) (Cummins and Pusey 1977).

Expansion of the exponentials in (6.6) leads to an effective field correlation function given by:

$$\begin{aligned}\ln g^{(1)}(K,\tau) = {}& \tfrac{1}{2}\ln[c(1+x+B)] - K^2(a\tau - d\tau^{1/2})(1-\tfrac{1}{2}x-B)\\ & + K^4(a^2\tau^2 - 2ad\tau^{3/2} + d^2\tau)(\tfrac{1}{4}x+B) + \ldots.\end{aligned} \tag{6.8}$$

For values of a and d relevant to this experiment, it can be shown that the $d^2\tau$ term is always negligible and that the $a^2\tau^2$ term is always larger than the $2ad\tau^{3/2}$ term when they are not both negligible compared with $a\tau - d\tau^{1/2}$. Thus the two main effects of heterodyning, number fluctuations and dust are (i) that the τ and $\tau^{1/2}$ terms in $\ln g^{(1)}$ are *reduced by the same fractional amount* and (ii) that a *positive* τ^2-dependent term becomes appreciable; the second cumulant (see equation (5.1)) associated with this term is $Q = (\frac{1}{2}x + 2B)$.

Some remarks concerning the expected magnitude of number fluctuations are in order here. Our sample preparation procedure, which involves shaking a diluted stock dispersion (§ 3.1), is unlikely to produce a uniform number density of particles. The time taken for uniformity to be achieved throughout the sample by diffusion is many days so that density variations on the scale of the scattering volume which remain when

residual flows in the sample have ceased are essentially 'frozen in'. The main cause of fluctuations in the number of particles in the scattering volume is then sedimentation. The time taken by a particle to sediment through the laser beam in a 40% D_2O/60% H_2O mixture is about 10^4 s (10 experiments of 10^3 s duration). Thus the population of particles changes by only about 10% during a single experiment. These rough calculations are supported by analysis of the total photon count (proportional to the number density) during 36 consecutive 10^3 s experiments. The average run-to-run variation in count was about 3% whereas the difference between the largest and smallest count observed was about 40%. We conclude therefore that large number density variations (of magnitude much greater than unavoidable Poisson variations expected with an otherwise uniform density) are frozen in but that the variation in number of particles in the scattering volume during a single 10^3 s experiment is about 3%. The constant B in equation (6.6) is the square of the relative number fluctuation so that we expect $B < 0.0009$. This prediction is confirmed by the observation (§ 5.2) of a long-delay-time value of $g^{(2)}(\tau)$ of 1.0007. Thus the considerations of this section, combined with the small expected and observed values of B, indicate that the effect of number fluctuations should be negligible in our experiments.

If $B = 0$, equation (6.8) applies to the case of pure heterodyning. Then, taking $x = 0.08$, for example, gives an apparent reduction in diffusion coefficient a of 4% (roughly the difference observed between experimental and theoretical values (§ 4)) and a second cumulant Q of 0.04.

6.5. Back reflections

With the optical geometry of figure 2 (with the sample cell vertical) there will be two back-reflected laser beams from the sample (water)–glass and glass–water bath interfaces of combined intensity 0.72% of the intensity of the main beam. The detector will therefore receive a small additional signal scattered by the sample at the complementary scattering angle $\theta' = 180° - \theta$. The extra distance, about 1 cm or less, travelled by the back-reflected beams is less than the expected coherence length of the laser light so that the main and additional signals will mix coherently. Thus we have

$$g^{(1)}(K, \tau) = (1-x)\,\mathrm{e}^{-Y_1} + x\,\mathrm{e}^{-Y_2} \tag{6.9}$$

where

$$Y_1 = K_1^2(a\tau - d\tau^{1/2})$$

$$Y_2 = K_2^2(a\tau - d\tau^{1/2})$$

and K_1 and K_2 are the scattering vectors appropriate for scattering angles θ and θ' respectively. Then

$$\begin{aligned}\ln g^{(1)}(K, \tau) &= -[(1-x)Y_1 + xY_2] + \tfrac{1}{2}x(1-x)(Y_1 - Y_2)^2 + \ldots \\ &= -[(1-x)K_1^2 + xK_2^2](a\tau - d\tau^{1/2}) + \tfrac{1}{2}x(1-x)(K_1^2 - K_2^2)^2 a^2\tau^2 + \ldots.\end{aligned} \tag{6.10}$$

Again the τ and $\tau^{1/2}$ terms are changed by the same fractional amount and a positive τ^2 term is found with a normalised second cumulant of $x[1-(K_2^2/K_1^2)]^2$ (for $x \ll 1$).

It is seen from figure 1 that the scattering powers of the particles are similar at $\theta \approx 65°$ and $\theta \approx 115°$ so that, for simplicity, we take $x = 0.0072$. Then for $\theta = 118°$ ($\theta' = 62°$) the τ and $\tau^{1/2}$ terms are reduced by a factor 0.995 whereas for $\theta = 66°$ ($\theta' = 114°$) they are increased by a factor 1.0099. The associated normalised second cumulants are 0.0029 and 0.0135 respectively.

6.6. Polydispersity and dimerisation

As discussed in § 3.1, the Mie scattering results indicate that the degree of polydispersity of the particles is small, with the standard deviation/the mean, $\sigma < 0.03$. Such a small degree of polydispersity will barely affect the average diffusion coefficient and will provide a negligible contribution, of the order of σ^2, to the second cumulant.

However particles as large as those used here can, under some conditions, exhibit reversible aggregation. The situation when a fraction (assumed small) of the particles is in the form of dimers can also be described by equation (6.9) with

$$Y_1 = K^2(a\tau - d\tau^{1/2}) \qquad Y_2 = K^2(a'\tau - d'\tau^{1/2}) \tag{6.11}$$

where a' and d' are the coefficients appropriate for the dimers. From (6.10) we get

$$\ln g^{(1)}(K, \tau) = -K^2\{a\tau[1 - x(1 - a'/a)] - d\tau^{1/2}[1 - x(1 - d'/d)]\}$$
$$+ \tfrac{1}{2}K^4 x(1-x)(a-a')^2\tau^2 + \ldots \tag{6.12}$$

with normalised second cumulant $Q = x(1 - a'/a)^2$.

We assume the diffusion coefficient a' of the dimer to be 0.7 times that of the monomer, a. Then taking $x = 0.1$, for example, gives an apparent reduction in diffusion coefficient of 3% and a second cumulant $Q = 0.009$. We note from equation (4.2) that the coefficient d of $\tau^{1/2}$ is independent of particle radius though, presumably, there is some shape dependence. Nevertheless it seems unlikely from the form of equation (6.12) that dimerisation would cause a greater reduction in d than in a.

It should also be mentioned that the dispersion, illuminated by laser light, was observed through a microscope. The individual particles were easily resolved and there was no evidence of a significant degree of dimerisation or higher-order polymerisation.

6.7. Multiple scattering

The theory outlined in § 2.1 and the subsequent data analysis are based on the first Born approximation, i.e. on the assumption that double and higher-order multiple scattering are negligible compared with single scattering. Two simple indications of the importance of multiple scattering in experiments of the type considered here are the degree of attenuation of the laser beam by the sample and the amount of depolarised scattering. For a weak scattering medium, the fraction F of incident intensity transmitted by the sample is close to one (if absorption is negligible). The probability of a single scattering is then roughly $1 - F$ and the probability of a double scattering roughly $(1 - F)^2$ so that the ratio of the intensities of double and single scattering is also about $1 - F$. When the incident beam is polarised so that its electric vector is perpendicular to the scattering plane (as in the present experiments) single scattering by isotropic spheres also has this polarisation and depolarised scattering can only arise from multiple-scattering events. (Nevertheless, the intensity of *polarised multiple* scattering may be several times that of depolarised multiple scattering (Sorensen *et al* 1976).) For the sample discussed in § 4 we found $1 - F \approx 0.1$ and the ratio of polarised to depolarised intensities at $\theta = 118°$ to be about 0.006. These observations indicate that the fraction of the total intensity detected in our experiments which is multiple scattered could well be several per cent.

Even in simple situations the theory of dynamic multiple scattering is quite complicated and there appears to have been no theoretical work on large spheres showing single-scattering patterns as complicated as that of figure 1. We are thus forced

to make experimental estimates of the effects of multiple scattering. To this end photon correlation measurements were made on a sample at number density $N \sim 5.6 \times 10^6$ cm^{-3} (about twice the concentration of the sample discussed in § 4) with the sample cell in two orientations, with either its long axis (1 cm) or its short axis (0.2 cm) parallel to the beam. Multiple scattering is expected to be more important in the former configuration since then the beam has travelled further through the sample to the scattering volume.

Table 5 lists the results of these experiments (made at $\theta = 118°$, $\lambda_0 = 4579$ Å and $T_S = 10$ μs) and, for comparison, similar experiments already discussed in §§ 4 and 5.4.

Table 5. The effect of multiple scattering.

Sample	Axis	Number density (cm^{-3})	Attenuation length (cm) (equation (3.2))	Relative intensity at centre of cell	Depolarisation ratio (%)	D (cm^2 s^{-1})	d (cm^2 s$^{-1/2}$)	$\frac{d_{exp}}{d_{th}}$
1	Long (1 cm)	5.6×10^6	1.0	0.61	3.8	1.138×10^{-9}	1.82×10^{-12}	0.85
1	Short (0.2 cm)	5.6×10^6	1.0	0.90	1.8	1.115×10^{-9}	1.49×10^{-12}	0.70
2 (§ 4)	Short	2.7×10^6	2.1	0.95	0.6	1.101×10^{-9}	1.58×10^{-12}	0.74
3 (§ 5.4)	Short	1.9×10^6	3.0	0.97	Not measured	1.194×10^{-9}[a]	1.61×10^{-12}	0.68

[a] Measured in 100% H_2O. Multiplication by viscosity ratio for comparison with other values in this table gives $D = 1.101 \times 10^{-9}$ cm^2 s^{-1}.

For simplicity we show only the coefficients of the 'long-time tail' fit (equation (4.1*c*)). Inspection of these results shows that, for the three experiments (2–4) for which the intensity of the illuminating beam at the centre of the scattering volume is greater than 90% of the incident intensity, the coefficients a and d (corrected where necessary to the same conditions) are the same within experimental error. Thus, although the concentration in experiment 2 was about three times greater than in experiment 4, there is no evidence that the increased multiple scattering (expected also to be about a factor of three greater) in the former case has caused significant distortion of the correlation function. By contrast, in experiment 1 where a much larger degree of attenuation is found both a and d are significantly higher than their low-concentration values.

For sample 1 the depolarised scattered intensity was strong enough for rough measurements to be made of its correlation function. With the long sample axis parallel to the beam semilogarithmic plots of the correlation function showed distinct upward curvature at large delay times and the effective diffusion coefficient (obtained from the initial slope) was as much as 1.5 times greater than the value found for the total scattering. In the short-axis configuration the log correlation function at $\theta = 66°$ also showed significant curvature though, at $\theta = 118°$, the log plot was almost linear with an effective diffusion coefficient only about 20% higher than the expected value.

We conclude that, although some multiple scattering is definitely present in our experiments, its effect on the quantities derived from the measurements appears to be small. It is nevertheless possible that the positive second cumulants observed may be caused, in part, by multiple scattering.

6.8. Interparticle interactions

The number density of the sample discussed in § 4 was $N \approx 2.7 \times 10^6\ \mathrm{cm}^{-3}$. Thus the fraction of the suspension volume occupied by the particles was about 6.3×10^{-5}; the mean distance between particles was about $N^{-1/3} \approx 72\ \mu\mathrm{m}$, some twenty particle diameters. It seems extremely unlikely that interparticle interactions would have a significant effect in such a dilute suspension. It is, in any case, worth noting that the measurements were made at scattering vectors well above those at which significant structure, caused for example by long-ranged Coulombic repulsions, would be found in the structure factor. Under these conditions light scattering observes effectively free-particle diffusion over distances short compared with the interparticle spacing (Pusey 1978).

6.9. Wall effects

It is well known that particle motions in a fluid are hindered by the presence of a wall (e.g. Happel and Brenner 1973). Typically the degree of hindering is of the order of the ratio of the particle radius to its distance from the wall. If the image of the slit (figure 2) formed in the sample by lens L2 is centred in the cell (§ 3.2) no particle 'seen' by the detector should be closer to a cell wall than about 250 μm (about 150 particle radii). It is possible however that due to diffraction, defocus or misalignment some particles close to the walls could contribute to the detected signal. Nevertheless, the vast majority of the particles observed should be effectively unhindered and any wall effects are expected to be small.

7. Summary and discussion

The important conclusion of this work is that figures 3 and 4 show clearly the existence of a long-time tail in the autocorrelation function of the velocity of a Brownian particle. Data obtained at short correlation delay times, where long-time tail effects are most marked, are summarised in table 6 and are completely consistent within themselves. However the experimental amplitude d of the long-time tail term is only about $74 \pm 3\%$ of that predicted theoretically (table 6, last column). When all the data are reviewed there are two main indications of systematic errors: (i) the value, 1.76 μm (after back-reflection corrections, § 6.5), of the particle radius calculated from the long-time

Table 6. Summary of short-delay-time results.

	T_S (μs)	θ (deg)	λ (Å)	Solvent	D ($\mathrm{cm}^2\,\mathrm{s}^{-1}$)	Radius (μm)	Coefficient d of $\tau^{1/2}$ (4.1c) ($\mathrm{cm}^2\,\mathrm{s}^{-1/2}$)	$\frac{d_{\mathrm{exp}}}{d_{\mathrm{th}}}$
§ 4	2, 5, 10 (averaged)	118	4579	60% H_2O 40% D_2O	1.101×10^{-9} (0.004)	1.77 (0.01)	1.58×10^{-12} (0.05)	0.74 (0.03)
§ 5.3	5, 10 (averaged)	66	4579	60% H_2O 40% D_2O	1.122×10^{-9} (0.005)	1.75 (0.01)	1.61×10^{-12} (0.12)	0.75 (0.06)
§ 5.4	10	116	6471	100% H_2O	1.194×10^{-9} (0.007)	1.77 (0.01)	1.61×10^{-12} (0.17)	0.68 (0.07)

diffusion coefficient determined by dynamic light scattering was about $4 \pm 2\%$ larger than that, 1.69 μm, determined by Mie scattering (§ 3.1); (ii) measurements made at longer delay times (§ 5) showed a slight upward curvature in the log correlation functions (a positive second cumulant). Several commonly encountered systematic errors (§ 6) could explain these findings and it seems likely that the observed discrepancies are caused by a combination of such errors. Unfortunately the full data analysis which revealed these discrepancies was not performed until after completion of the experiment so it was not possible to investigate further the individual systematic errors. In any case the requirements of the experiment precluded simultaneous minimisation of all sources of error. For example, the use of large particles (for a large long-time tail effect, § 2.3) leads to significant multiple scattering which can only be minimised by use of a small sample volume, a requirement also indicated to avoid convection. However such a small volume allows the possibility of the detection of light scattered elastically by the cell walls, which can also hinder the particle motions. Nevertheless, *it should be emphasised* that none of the systematic errors considered in § 6 appears to explain the fact that the disagreement between experiment and theory is much larger for d (the amplitude of the long-time tail term) than for the diffusion coefficient D.

In view of the smallness of the effect investigated and the abovementioned difficulties it would be foolish to claim categorically that a real difference between experiment and theory has been found: it is entirely possible that the discrepancy observed could be caused by some unidentified artefact. Nevertheless it is worth considering briefly where failings in the theory could be sought. Firstly we note that, in obtaining (2.6) from (2.3), we have assumed, in accordance with the usual theories of Brownian motion (Dufty 1974, Fox 1977), that the particle velocity v is a Gaussian-distributed random variable (see, however, Dufty and McLennan 1974). In fact, if measurements are made at short times (as in § 4), such an assumption is not necessary since expansion of (2.3) gives

$$g^{(1)}(K, \tau) = 1 - \tfrac{1}{2}K^2\langle \Delta x^2(\tau)\rangle + \ldots \tag{7.1}$$

regardless of the statistics of v. Thus non-Gaussian effects contribute only to higher-order terms in (7.1). The consistency of the data obtained at different (short) sample times (table 1) tends to support the unimportance of possible non-Gaussian effects. Secondly, the theory outlined in § 2 and the appendix is based on the application of macroscopic hydrodynamics to the microscopic Langevin equation. Since the particle radius is some 10^4 times greater than typical molecular sizes this approach seems reasonable. Nevertheless it should be noted that theories which start closer to first principles (see e.g. Pomeau and Résibois 1975) are less categorical in their predictions (although the theoretical amplitude of the $t^{-3/2}$ term in $\phi(t)$ seems well established). If the theoretical approach used here is accepted then our results, if correct, must be seen as disagreeing with macroscopic theories of unsteady, low Reynolds number hydrodynamic flows. While we have not searched the literature in detail, one assumes that these theories have been well tested experimentally on such macroscopic phenomena as starting flow in a pipe (e.g. Batchelor 1967, p 193). Certainly authors of modern textbooks on fluid dynamics do not seem to feel the need to cite much experimental confirmation of the theory.

Finally we compare our results with other experiments on Brownian particles. The light-scattering results of Bouiller *et al* (1978) include in their error bracket both the theoretical prediction and our findings for the amplitude of the long-time tail term and

are therefore not inconsistent with either. Fedele and Kim (1980), by direct observation of a single Brownian particle suspended in a gas, found a long-time tail of amplitude *greater* than that predicted theoretically. It is not easy, from their report, to determine error estimates which can be compared with ours.

In conclusion, solid experimental evidence has been found for the existence of a long-time tail; significant disagreement between the experimental and theoretical magnitudes remains.

Acknowledgments

We are extremely grateful to Professor R H Ottewill for providing both the large monodisperse polystyrene spheres which made this experiment possible and the computer program used to generate the theoretical Mie scattering profiles. PNP is pleased to acknowledge several valuable discussions in 1971 with Professors B J Berne and D E Koppel on the subject of long-time tails and light scattering. We thank Dr R J A Tough for the calculations reported in the appendix and Dr R B Jones for a useful discussion.

Appendix

Laplace transformation of the modified Langevin equation (2.11) gives for $\tilde{\phi}(s)$, the transform of the velocity autocorrelation function (e.g. Hinch 1975),

$$\tilde{\phi}(s) = \int_0^\infty \exp(-st)\phi(t)\,\mathrm{d}t$$
$$= D[1+(sR^2/\nu)^{1/2}+(sR^2/9\nu)(1+2\rho_P/\rho)]^{-1} \tag{A1}$$

where the kinematic viscosity $\nu = \eta/\rho$. We see immediately that

$$\tilde{\phi}(0) = \int_0^\infty \phi(t)\,\mathrm{d}t = D.$$

(A1) can be inverted by integration about a Bromwich contour in the s plane, cut along the real axis from $-\infty$ to 0 (e.g. Jeffreys and Jeffreys 1972, ch 12) to give

$$\phi(t) = \frac{RD}{\pi\nu^{1/2}}\int_0^\infty \mathrm{d}p\, p^{1/2}\exp(-pt)(1+\alpha p+\beta p^2)^{-1} \tag{A2}$$

where

$$\alpha = (R^2/9\nu)(7-4\rho_P/\rho) \qquad \text{and} \qquad \beta = (R^2/9\nu)^2(1+2\rho_P/\rho)^2.$$

While it is possible to reduce this result to a closed form (e.g. Hinch 1975), the $t\to\infty$ asymptotic behaviour of $\phi(t)$ and the related quantities $D(\tau)$ and $\langle\Delta x^2(\tau)\rangle$ are most readily obtained directly from their integral representations. Watson's lemma (Copson 1972, p 218) allows us to write

$$\phi(t) = \frac{RD}{\pi\nu^{1/2}}\int_0^\infty \mathrm{d}p\, p^{1/2}\exp(-pt)[1-\alpha p+(\alpha^2-\beta)p^2]+\mathrm{O}(t^{-9/2})$$

from which (2.12) follows immediately; we note that for $\rho = \rho_P$ the $t^{-7/2}$ term vanishes identically. $D(\tau)$, the time-dependent diffusion coefficient (2.16), can be cast in suitable form for asymptotic development as follows:

$$D(\tau) = \int_0^\tau \mathrm{d}t\, \phi(t)$$

$$= \frac{RD}{\pi\nu^{1/2}} \int_0^\infty \mathrm{d}p\, p^{-1/2}[1-\exp(-p\tau)](1+\alpha p+\beta p^2)^{-1}$$

$$= \frac{RD}{\pi\nu^{1/2}}\left(\int_0^\infty \mathrm{d}p\, p^{-1/2}(1+\alpha p+\beta p^2)^{-1} - \int_0^\infty \mathrm{d}p\, p^{-1/2}\exp(-p\tau)\right.$$

$$\left. + \int_0^\infty \mathrm{d}p\, p^{-1/2}\exp(-p\tau)(\alpha p+\beta p^2)(1+\alpha p+\beta p^2)^{-1}\right). \tag{A3}$$

On evaluating the first and second of these integrals and developing the asymptotic form of the third we obtain (2.17). The mean-square displacement $\langle \Delta x^2(\tau)\rangle$ can be found similarly by noting that

$$\langle \Delta x^2(\tau)\rangle = 2\int_0^\tau D(t)\,\mathrm{d}t. \tag{A4}$$

(2.14) follows from substitution of (A3) in (A4) and an integration by parts.

References

Alder B J and Wainwright T E 1967 *Phys. Rev. Lett.* **23** 988–90
—— 1968 *J. Phys. Soc. Japan Suppl.* **26** 267
—— 1970 *Phys. Rev.* A **1** 18–21
Andriesse C D 1970 *Phys. Lett.* **33A** 419–20
Batchelor G K 1967 *An Introduction to Fluid Dynamics* (Cambridge: Cambridge University Press)
Boon J P and Bouiller A 1976 *Phys. Lett.* **55A** 391–2
Bosse J, Götze W and Lücke M 1979 *Phys. Rev.* A **20** 1603–7
Bouchiat M A and Meunier J 1971 *J. Physique* **32** 561
—— 1972 *J. Physique* **33** Colloque C-1 141–8
Bouiller A, Boon J P and Deguent P 1978 *J. Physique* **39** 159–65
Carneiro K 1976 *Phys. Rev.* A **14** 517–20
Copson E T 1972 *Theory of Functions of a Complex Variable* (Oxford: Clarendon)
Cummins H Z and Pike E R 1974 *Photon Correlation and Light-Beating Spectroscopy* (New York: Plenum)
—— 1977 *Photon Correlation Spectroscopy and Velocimetry* (New York: Plenum)
Cummins H Z and Pusey P N 1977 in *Photon Correlation Spectroscopy and Velocimetry* ed H Z Cummins and E R Pike (New York: Plenum) pp 164–99
Davenport W B and Root W L 1958 *Random Signals and Noise* (New York: McGraw-Hill) pp 50, 145
Dufty J W 1974 *Phys. Fluids* **17** 328–33
Dufty J W and McLennan J A 1974 *Phys. Rev.* A **9** 1266–72
Fedele P D and Kim Y W 1980 *Phys. Rev. Lett.* **44** 691–4
Fox R F 1977 *J. Math. Phys.* **18** 2331–5
Fuller G G, Rallison J M, Schmidt R L and Leal L G 1980 *J. Fluid Mech.* **100** 555–75
Happel J and Brenner H 1973 *Low Reynolds Number Hydrodynamics* (Leiden: Noordhoff)
Harris S 1975 *J. Phys. A: Math. Gen.* **8** L137–8
Hinch E J 1975 *J. Fluid. Mech.* **72** 499–511
Jakeman E 1975 *J. Phys. A: Math. Gen.* **8** L23–8
Jeffreys H and Jeffreys B 1972 *Methods of Mathematical Physics* (Cambridge: Cambridge University Press)
Jones R B 1980 *Physica* **101A** 389–406

Kerker M 1969 *The Scattering of Light and Other Electromagnetic Radiation* (New York: Academic)
Kim Y W and Matta J E 1973 *Phys. Rev. Lett.* **31** 208–11
Landau L D and Lifshitz E M 1966 *Fluid Mechanics* (Oxford: Pergamon)
Nelkin M 1972 *Phys. Fluids* **15** 1685–90
Oliver C J 1974 in *Photon Correlation Spectroscopy and Velocimetry* ed H Z Cummins and E R Pike (New York: Plenum) pp 151–223
Pomeau Y and Résibois P 1975 *Phys. Rep.* **19** 63–139
Pusey P N 1978 *J. Phys. A: Math. Gen.* **11** 119–35
—— 1979 *Phil. Trans. R. Soc.* A **293** 429–39
Pusey P N, Koppel D E, Schaefer D W, Camerini-Otero R D and Koenig S H 1974 *Biochemistry* **13** 952–60
Smithsonian Physical Tables 1964 ed W E Forsythe (Washington: Smithsonian Institution)
Sorensen C M, Mockler R C and O'Sullivan W J 1976 *Phys. Rev.* A **14** 1520–32
Uhlenbeck G E and Ornstein L S 1930 *Phys. Rev.* **36** 823–41
Warner M 1979 *J. Phys. A: Math. Gen.* **12** 1511–9
Wax N ed 1954 *Selected Papers on Noise and Stochastic Processes* (New York: Dover)
Widom A 1971 *Phys. Rev.* A **3** 1394–6
Zollweg J, Hawkins G and Benedek G B 1971 *Phys. Rev. Lett.* **27** 1182–5
Zwanzig R and Bixon M 1970 *Phys. Rev.* A **2** 2005–12
—— 1975 *J. Fluid. Mech.* **69** 21–5